Soft Matter

Accepted Manuscript

This is an *Accepted Manuscript*, which has been through the Royal Society of Chemistry peer review process and has been accepted for publication.

Accepted Manuscripts are published online shortly after acceptance, before technical editing, formatting and proof reading. Using this free service, authors can make their results available to the community, in citable form, before we publish the edited article. We will replace this *Accepted Manuscript* with the edited and formatted *Advance Article* as soon as it is available.

You can find more information about *Accepted Manuscripts* in the Information for Authors.

Please note that technical editing may introduce minor changes to the text and/or graphics, which may alter content. The journal's standard Terms & Conditions and the Ethical guidelines still apply. In no event shall the Royal Society of Chemistry be held responsible for any errors or omissions in this *Accepted Manuscript* or any consequences arising from the use of any information it contains.

ROYAL SOCIETY OF CHEMISTRY

www.rsc.org/softmatter

We used a reactor-like spinneret to generate a continuous hollow alginate fiber and investigated the interfacial deformation dynamics.

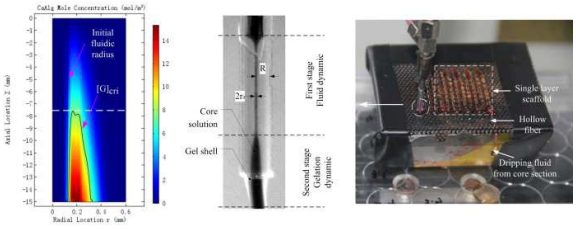

Soft Matter Accepted Manuscript

Journal Name

ARTICLE

Reactor-like spinneret used in 3D printing alginate hollow fiber: numerical study of morphological evolution

Received 00th January 20xx,
Accepted 00th January 20xx

DOI: 10.1039/x0xx00000x

www.rsc.org/

Y. Li,[ab] Y. Liu,*[a] C. Jiang,[a] S. Li,[a] G. Liang[a] and Q. Hu[a]

In this paper, a reactor-like spinneret is proposed to generate a continuous hollow hydrogel fiber. In order to reliably control the deforming dynamics, the components of the spinneret are standardized in order to ease the online observation of morphological evolution. We found that not only did a co-flow occur in the tubular space, but a relatively large shrinkage of the shell layer at the outlet also occurred. Whereupon a weak coupling of the velocity field and diffusion-reacting co-flow was developed to describe the monitored co-flow morphology and to simulate the intermediate state of the concentration field, as well as to calculate the shrinkage profile with an integral formula. And a critical isogram $[G]_{\mathrm{cri}}$ was determined to correspond to the morphological segmental feature, to trigger gelation and shrinkage as a threshold of solubility and the integral upper limit of the shrinkage region. Experimental evidence indicates that: the simulation is able to effectively predict the inner diameter of the hollow fiber; the transient inner diameter of the fiber at the outlet is expanded by approximately 70μm (co-flow distance=15mm) as compared to the initial fluid dynamics value, and that the relative mean error of the simulated inner diameter was less than 8%. The proposed study provides deeper insight into the printing of hollow fibers and other gelling processes which utilize a reactor-like spinneret.

1 Introduction

Alginates are anionic polysaccharides composed of β-D-mannuronic acid and α-L-guluronic acid, a popular biomaterial due to its convenient sources, nontoxicity, and excellent biocompatibility and biodegradability[1,2]. Moreover, 3D printing is considered a core technology related to biofabrication, a well-known "bottom-up" technique. As a carrier of drugs and cells with a certain geometry via 3D printing, alginate is highly applicable to the field of tissue engineering, as well as to pharmaceutical and clinical medicine[3,4].

The reactor-like spinnerets offer a way to tie the 3D printing technique and the crosslinkable materials effectively together, and to expand the solidification mechanism used in 3D printing (especially for free deposit forming mode) from conventional temperature control into chemical reaction. In contrast to traditional external gelation[5-7], the preparation of alginate hollow fibers is developed from the fabrication of hydrogel microspheres on coaxial microfluidics[8,9], which is a novel attempt to address the vascularization[10,11] of tissue engineering scaffolds in vivo. Since the spinneret was simplified from a triple-orifice spinneret[12,13] to a double-orifice spinneret[8,14], it has provided a relatively drier environment for the direct construction of particular architectures.

Since the ion diffusion which induced crosslink has interactions with the geometric size and viscosities of the co-flow, the gelling process is very complicated and has not yet been studied extensively. But the demands on products have transferred from the formation of shapes and complete crosslinking to pursuing accuracy control of the gel process. Some researchers investigated fluid dynamics as a single control mechanism for the reacting co-flow[5], but neglected to account for shrinkage which has behaved its importance in the study of alginate microspheres and film in static water baths[5,6]. This neglect may be suitable for solid fibers, but shrinkage will significantly influence the size of the wall thickness of hollow fibers, thus affecting the structural strength of hollow fibers as well as the diffusion environment of embedded cells and drugs. In actuality, the experimentally observed inner diameter is much greater than the fluidic calculated value, which necessitates investigation into the morphological evolution and mechanism.

To address the aforementioned disadvantages, the spinneret structure was redesigned based upon the spinneret of Ibrahim T. Ozbolat[8] in order to not only generate a $CaCl_2$-in-alginate coaxial microfluidic but to also introduce the potential for industrialization and standardization. Then, with the aid of the modified spinneret, the co-flow state was carefully monitored online, and the forming dynamics were modelled and analysed. Finally, the dimensions of the printed hollow fiber were compared to simulated results to verify the effectiveness of the proposed weak coupling formulas.

[a] Rapid Manufacturing Engineering Center, Shanghai University, Shanghai 200444, China. E-mail: Yuanyuan_liu@shu.edu.cn
[b] School of Mechanical and Power Engineering, Henan Polytechnic University, Jiaozuo, Henan 454000, China.
[c]

Soft Matter Accepted Manuscript

2 Materials and methods

2.1 Materials

Sodium alginate (chemically pure, molecular weight of approximately $3.5 \times 10^7 g\ mol^{-1}$) and calcium chloride ($CaCl_2$) (analytically pure, molecular weight 110.8 $g\ mol^{-1}$) were used to fabricate the hydrogel fiber. First, 3~5% (w/v) sodium alginate was dissolved in deionized water and placed in a shaker at room temperature for 10 hours at 120 rpm. Additionally, 2~4% (w/v) $CaCl_2$ solution was similarly prepared with deionized water. All of the above reagents were purchased from the Sinopharm Chemical Reagent Co. (China).

2.2 Reactor-like spinneret

In the present study, a reactor-like spinneret was introduced to generate a $CaCl_2$-in-alginate coaxial microfluidic. As shown in Figure 1a, the preparation process can be separated into three steps (α-γ). In the α region, the sodium alginate solution is dispensed through the shell section of the coaxial spinneret, while the calcium chloride solution is dispensed through the core section. In the β region, the two solutions are dispensed out of the spinneret; when the two solutions come into contact with one another, crosslinking occurs. Moreover, with the radial diffusion of calcium ions from inner to outer, the shell gradually gelates in the direction of the flow. Finally, in the γ region, the hollow fiber is deposited and forms a particular shape on the receive board under the control of motion units.

As shown in Figure 1b, the spinneret consists of four parts: the inner nozzle, outer nozzle, T-cock, and quartz tube. According to the empirical clog distance, the outer needle was shorter than the inner needle ($\Delta l = 5$ mm); a quartz tube of a certain length was used to equip and lengthen the outer needle, to form a tubular reactor. The reactor-like spinneret offer several advantages: 1) The spinneret is inexpensive, easily manufactured, and its specifications are easily altered; 2) Hydrogel that has clogged the orifice can be conveniently removed by the detachment of components; 3) The quartz tube allows for observation of co-flow fluids, similar to the function of a PDMS microfluidic chip in other works[16, 17]; 4) The quartz tube can additionally convert extrusion swelling of the hydrogel from the radial direction to the axial direction, and the outer diameter of the hollow fiber is uniform; 5) Disturbances to the coaxial jet resulting from environment factors are largely eliminated.

Experiments were conducted on a 3D biological printing platform (home-built equipment, Shanghai University, China), as shown in Figure 1c. The printing platform consisted of a tri-axial motion unit, a CAD/CAM software unit, and a multimode feed unit. The alginate sol and the calcium chloride solution were both dispensed by syringe pumps. The core fluid dripped constantly at the beginning of the hollow fiber, as shown in Figure 1d. Moreover, this phenomenon also proves the unblocked hollow structure of the printed fiber.

2.3 Morphology study

Morphological evolution was monitored online with a high speed CCD camera (CMLN-13S2M, PointGrey, Canada). The dimensions of the printed hollow fiber were verified by optical microscopy (EV3020, EASSON, China). The cross-sectional features of the hollow fiber were also observed by SEM (SU1510, Hitachi, Japan). The tubular fiber was first dehydrated with Hexamethyldisilazane (HMDS) and anhydrous ethanol and then coated with a conductive layer for observation by SEM.

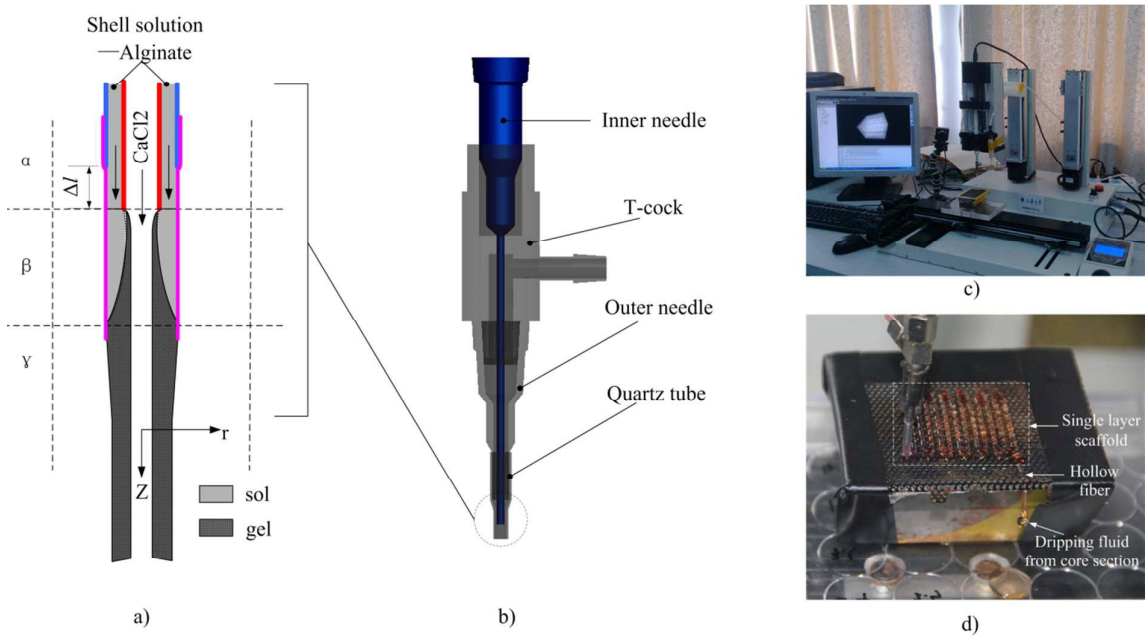

Fig. 1 Schematic of 3D printed hollow hydrogel fiber and scaffold. (a) $CaCl_2$-in-alginate coaxial microfluidic; (b) reactor-like spinneret; (c) biological 3D printing platform; (d) 3D printing status.

Soft Matter Accepted Manuscript

This journal is © The Royal Society of Chemistry 20xx

Journal Name

ARTICLE

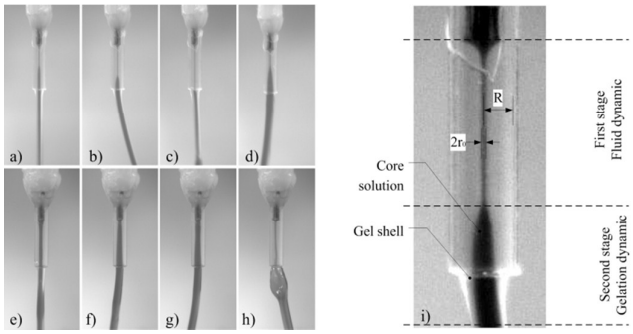

Fig. 2 On-line observation of extrusion states with dye tracer (a flow pattern sequence via various Q_c/Q_s μL/min). (a) 400/400; (b) 400/600; (c) 400/800; (d) 600/400; (e) 800/400; (f) 900/400; (g) 1000/400; (h) 200/400; (i) magnification of interfacial deformation; ($CaCl_2$: 3% (w/v), alginate: 4% (w/v)).

3 On line observation

The observation of the co-flow pattern during extrusion contributes to the overall understanding of the deformation dynamics. In order to better visualize the flow state, Rhodamine 6G dye was added to the $CaCl_2$ solution as flow tracer.

As shown in Figure 2a-h, a sequence of flow patterns was obtained by changing the dispensing rates of the core solution (Q_c, μl/min) and the shell sol (Q_s, μl/min). Flow patterns have been classified by Utada[19] for the two-phase flows (which are nonreactive with one another) as dripping, drag jetting, and ejection jetting. When the coupled crosslink-diffusion effect is taken into account as in the present study, the same flow patterns were observed with the exception of dripping; however, a clog occurred in the inner needle, as shown in Figure 2(h). The general requirements of hollow fibers are unobstructed lumens and uniform dimensions. Thus, the core solution ($CaCl_2$) should not be interrupted or dispersed during the co-flow time until the shell hydrogel had gelled completely. Accordingly, considering the mechanical requirements (i.e., wall thickness), drag jetting was identified as the appropriate choice (Figure 2a-d.).

As shown in Figure 2i, not only is a stable drag jetting created, which occupies most of the tube space, but a relatively large deformation at the outlet also occurs. Additionally, interfacial deformation began at the outlet of the spinneret and travelled upstream to a distance that varied depending upon the flow conditions. Interfacial deformation is likely a result of the gelation process, and an expansion of the inner diameter due to the radial shrinkage of the shell rather than diffusion of the dye. This phenomenon will be discussed in the following paragraphs.

4 Mathematical Model for Morphological evolution

4.1 Hypothesis

As demonstrated by the test results described above, the simple preparation technology of hollow fibers contains complex mechanisms which include not only a two-phase coaxial flow and a simultaneous reaction-diffusion process, but also include a continuous moving boundary as precipitation or membrane drying process do. In order to simplify this investigation, the following assumptions were applied:

1) Mass transfer was initially conducted after the velocity distribution was fully developed, rather than conducted concurrently.

2) It is subsequently assumed that the diffusion process does not change the velocity profiles or the fluid properties (viscosity, diffusion rate, etc.).

3) Gel formation is a precipitation-like reaction. The macromolecular chain contracts in the normal direction (outwards) of the flow in the transformation process of sol to gel, and the supersaturated water is transferred to the core. Thus, two lines are obtained: one representing the reaction front which is constrained by the diffusion of calcium ions, the other representing the shrinkage profile, which is proportional to the reaction zone and determines the instantaneous inner diameter of the hollow fiber.

4) Due to the short time of the extrusion process, migration of the sodium alginate macromolecular in the sol is ignored.

4.2 Velocity field of the co-flow

For the first stage, the co-flow morphology primarily follows the continuity and Navier–Stokes equations. Theoretical equations representing the core fluid diameter and velocity field were established as described by Eqn. (1) and (2), respectively[15,17].

$$\left(1+\frac{Q_c}{2Q_s}-\frac{\mu_s}{2\mu_c}\right)r_0^4-\left(1+\frac{Q_c}{Q_s}\right)R^2r_0^2+\frac{Q_c}{2Q_s}R^4=0 \qquad (1)$$

$$\begin{cases} v_z(r)=\frac{Q_c+Q_s}{\pi R^2}\cdot\left(\frac{\mu_s}{\mu_c}\cdot\frac{r^2-r_0^2}{R^2-r_0^2}-1\right), & if\ 0\le r\le \mathrm{r}_0 \\ v_z(r)=\frac{Q_c+Q_s}{\pi R^2}\cdot\frac{r^2-R^2}{R^2-r_0^2}, & if\ \mathrm{r}_0\le r\le R \end{cases} \qquad (2)$$

Where, r_0 is the radius of the core solution in the first stage; R is the inner radius of the quartz tube; μ_c and μ_s are the viscosities of the core and shell solution, respectively; Q_c and Q_s are the dispense rates of the core and shell solution, respectively; $v_z(r)$ is the velocity in axial direction as well as a function of *r*.

As a quartic implicit function, the Eqn. (1) points out the primary influence factors affecting r_0, such as flow rates ratio,

Soft Matter Accepted Manuscript

viscosity ratio and the diameter of the reacting space. And the Eqn. (2) presents the co-flow velocity field as a piecewise and nonlinear function.

4.3 Species transport in reactor-like spinneret

The gelation reaction involves specific carboxylic acid groups along the polymer chain which contains guluronic and mannuronic acids; only the former participates in the binding of Ca^{2+} ions into the gel whose topology has been described with the egg box model[19]. The crosslink reaction can be described as Eqn. (3):

$$nNaAlg_{monomer} + Ca^{2+} = CaAlg \quad (3)$$

The coefficient n is therefore calculated according to the composition of the alginate (only the acids belonging to the guluronic family are counted), its molecular weight, and the gelation model, etc. Here, we defined n=3.42 in agreement with T. Braschler[20]. The diffusion of these two species is therefore neglected in the equations describing the alginate and gel concentrations. Since, the species transport equation needs to be coupled with the flow equation (Eqn. (2)), the mass-balance equation for each species can be described as Eqn. (4):

$$\begin{cases} v_z(r)\cdot\frac{\partial[S]}{\partial z} = D\cdot\frac{1}{r}\frac{\partial}{\partial r}\left(r\cdot\frac{\partial[S]}{\partial r}\right) - R_S \\ v_z(r)\cdot\frac{\partial[A]}{\partial z} = -R_A \\ v_z(r)\cdot\frac{\partial[G]}{\partial z} = R_G \end{cases} \quad (4)$$

Where, $[S]$, $[A]$, and $[G]$ are the concentration of Ca^{2+}, Alg and CaAlg, respectively; R_S, R_A, and R_G are the reaction terms of the three species, respectively; D is the diffusion coefficient of Ca^{2+}; $\frac{\partial[*]}{\partial z}$ and $\frac{\partial[*]}{\partial r}$ are the concentration gradient of the three species in axial and radial directions, respectively.

4.4 Shrinkage profile

The shrinkage profile is proportional to the reaction zone, and the shrinkage ratio per unit volume λ can be determined by the swelling degree or colloid density[21-23]. The gel fraction G_{fra} can then be obtained according to the CaAlg concentration field. Therefore, the radial location of the shrinkage profile can be expressed as follows:

$$V_{final} \to \pi(r_r^2 - r_s^2) = \int_{r_0}^{r_r} \lambda\cdot 2\pi r\cdot G_{fra} + 2\pi r\left(1 - G_{fra}\right)dr \quad (5)$$

$$\text{i.e. } r_s = \sqrt{r_r^2 - 2\int_{r_0}^{r_r}\lambda\cdot r\cdot G_{fra} + r(1-G_{fra})dr}$$

$$\text{or } r_s = \sqrt{r_0^2 + 2\int_{r_0}^{r_r}(1-\lambda)\cdot r\cdot G_{fra}dr} \quad (6)$$

Where, V_{final} is the final volume of the shrunk portion; r_r is the radial location of the reaction front; and r_s is the radial location of the Shrinkage profile, i.e. the transient radius of the core solution.

5 Simulation results and discussions

5.1 Gelation process and gel fraction gradient

The geometry of the co-flow space is rotationally symmetric, and it is possible to reduce the model from 3D to a 2D axisymmetric problem. This means that we only have to model half of the tube cross section. In 2D axisymmetric (plane r, z), the representation of the co-flow is reduced to two simple rectangles (Region 1, 2), as seen in Fig.3a. The rectangles' width (r_0, $R - r_0$) are determined and parameterized with Eqn. (1); the velocity field of each region is set according Eqn. (2). Due to the huge viscosity change, there exists an obvious inflection point in the $v_z(r)$ curve. Upon weak coupling of the velocity field (Eqn. (2)) and diffusion of the reacting co-flow (Eqn. (4)), we obtain an intermediate state of concentration field, where the shell portion has not shrunk yet, as seen in Fig. 3b-d.

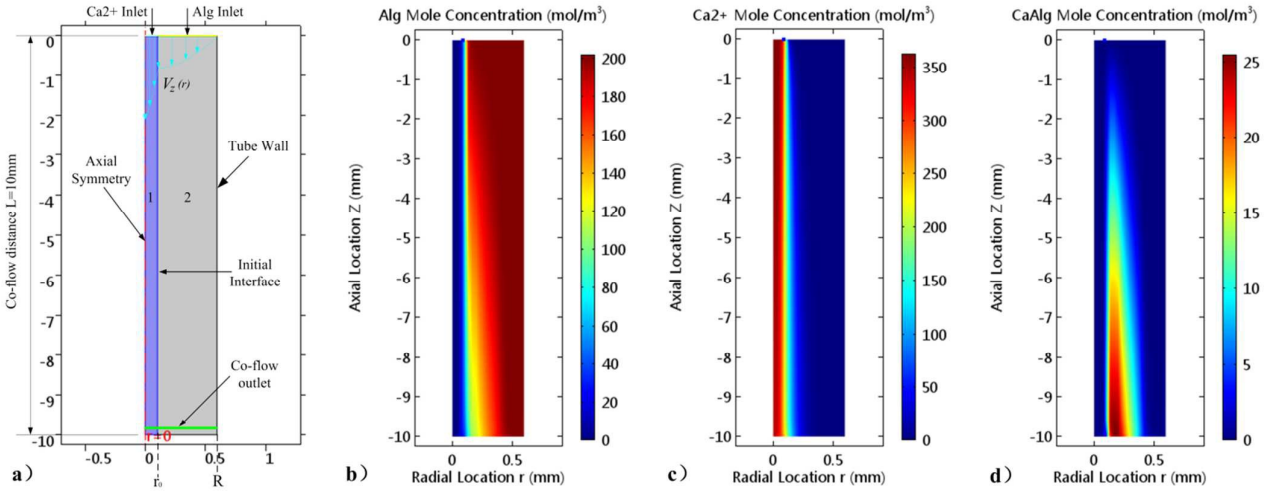

This journal is © The Royal Society of Chemistry 20xx

Please do not adjust margins
Soft Matter Accepted Manuscript

Fig. 3 Boundary conditions (a): Q_c=400 μL/min, Q_s=400 μL/min, Initial concentration $C_{Ca^{2+}}$ =360 mol/m^3, C_{Alg} = 202 mol/m^3; and simulated intermediate state of concentration field of alginate monomer (b), calcium ion (c), and CaAlg (d).

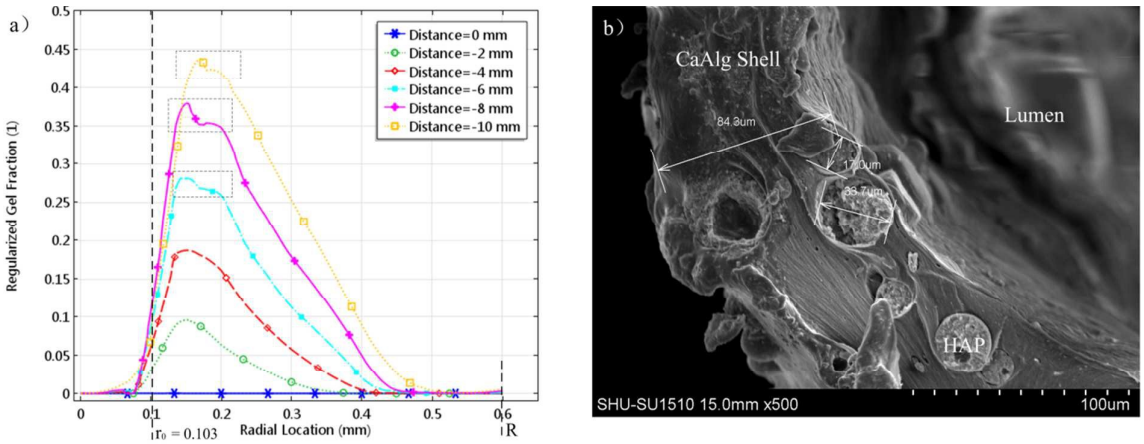

Fig. 4 Gel fraction gradient profile and feature inspection of printed fiber. (a) regularized gel fraction (G_{fra}) in radial direction at different co-flow distances; (b) layered texture of fiber wall, note that the hydroxyapatite microspheres (HAP) are an additional phase to inhibit shrinkage during the dehydration process.

The species concentration fields obtained with this calculation procedure: with the increase of co-flow distance, the distribution of Ca^{2+} progresses from the center of the co-flow jet to the shell portion gradually (Fig.3c), and Alginate is consumed upon Ca^{2+} diffusion (Fig.3b) as well as the CaAlg gel is created (Fig.3d), and the boundaries of the alginate and CaAlg do not move as expected from their neglected diffusion.

Fig.4a shows the profile of regularized gel fraction ($G_{fra} = n[G]/C_{Alg}$) along radial direction. We found that there is an increased maximum and gradient for the regularized gel fraction as the increase of co-flow distance (Fig.4a). More details, farther co-flow distance means longer crosslinking time，and the networks nearby initial interface becomes more dense; And there is a “step” in some G_{fra} profiles (Distance=-6, -8, -10mm) marked with dashed boxes in Fig. 4a. The variation tendency of the steps (increases first and then decreases) also reflect the accumulation of CaAlg gel. In practice, this gradient feature was also observed in SEM detection of the hollow fiber (Fig.4b). The layered texture of the shell becomes sparser gradually from inside to outside.

Note that since the diffusion direction of Ca^{2+} is vertical to the transfer direction of finite element calculation, the maximum G_{fra} drifts off the initial interface ($r_0 = 0.103mm$) and there is a bit of CaAlg gel fleeing to core, as seen in Fig. 4a. Therefore, the grid division near the initial interface should be meshed more tensely to improve the accuracy of the simulation.

5.2 Morphological evolution analysis

Calcium alginate hydrogels are widely used in various applications. However, it is difficult to control their reaction rates, dimensions, and homogeneity, particularly in dynamic and micro-scale processes. To overcome this problem, much research to date has primarily focused on model validation and simulation. First, the morphological evolution was simulated and the effects of extrusion conditions, such as co-flow distance and the inner and outer flow velocity, were analyzed.

Online monitoring images (Fig. 2i) demonstrated that the morphology could be divided into two typical portions, with distinct differences, which is in accordance with simulation results: the concentration isogram $[G]$ and the initial fluidic radius create a similar profile (Fig.5). This may indicate an inevitable inherent relationship between the two profiles. In agreement with Oriane Bonhomme[16], it is assumed that the gel formation represents a precipitation-like reaction: a given amount of salt is required to initiate gelation and above this point, the unbounded reactants are linked by a solubility product which fixes their concentrations. In other words, there is a critical CaAlg concentration value ($[G]_{\mathrm{cri}}$) which triggers gelation and shrinkage as well as represents the reaction front. $[G]_{\mathrm{cri}}$ was estimated with solubility experimental results, and a good compromise is found for $[G]_{\mathrm{cri}} = 7.8mol/m^3$. Before developing to the threshold $[G]_{\mathrm{cri}}$, the morphology of the co-flow is controlled solely by fluid dynamics, and the inner diameter remains unchanged. As the thickness of the gel layer increases, the inner diameter also expands, which originates from the condensation reaction. Consequently, the morphological evolution of the hollow fiber can be separated into two stages, and successively ascribed to fluid dynamics and gelation dynamics.

Soft Matter Accepted Manuscript

Please do not adjust margins

Journal Name

ARTICLE

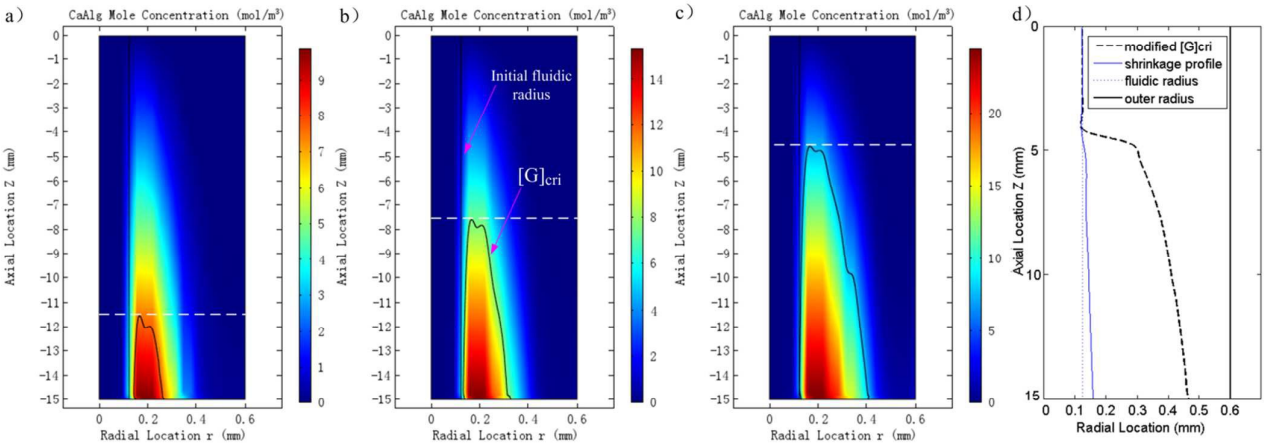

Fig. 5 Simulation of a sequence of flow states with a constant flow rate ratio Q_c/Q_s ($\times 10^{-2}$ mL/s) =0.5: (a) 15/30; (b) 11/22; (c) 6.7/13.4; (d) steady shrinkage profile calculated with the situations of Fig.5c; $[G]_{\mathrm{cri}} = 7.8mol/m^3$.

Co-flow distance has a positive effect on the thickness of gelled portion and the CaAlg concentration. As shown in Fig. 5a-c, greater co-flow distance indicates longer residence time, which increases gel thickness and gel fraction. Additionally, results indicate that gel thickness and gel fraction decreases as average co-flow velocity (with constant flow rate ratio) increases, which may be attributed to the lower residence time and gelation time. Therefore, these factors may be controlled to achieve precision control of the thickness of the gel layer or the residual sol layer by balancing the residence and gelation times.

However, the parabolic shape of concentration isogram $[G]$ is apparently not practical, also cannot precisely reflect the location of the reaction front. To avoid the distortion mentioned above, the critical concentration isogram $[G]_{\mathrm{cri}}$ was extracted and undergone a series of treatment firstly, such as segmentation and curve smoothing, to transform into a modified $[G]_{\mathrm{cri}}$; then, take the radial location of the modified $[G]_{\mathrm{cri}}$ contour as the integral boundary of Eqn. (6), we can calculate and depict the shrinkage profile, i.e. the steady interface of co-flow, as seen in Fig. 5d. It can be seen that the shrinkage profile is more approximate to the core flow pattern online observed. And we will verify the validity of the simulation results in the following section.

5.3 Verification on target objects

Geometric dimensions are closely related to the mechanical strength and diffusion range of the hydrogel hollow fiber, which is critical to the practical applications of cell and drug loading. Thus, the present study focuses on the transient dimensions of each physical object at the outlet, such as the inner diameter and residual sol thickness.

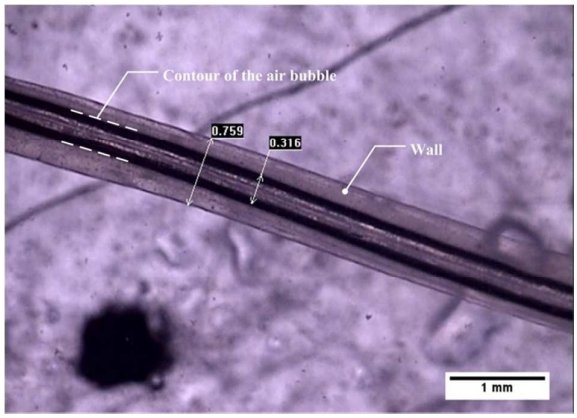

Fig. 6 Dimension measurement of printed hollow fiber under optical microscopy

Fig.6 shows a sample of printed fiber, the dimensions of hollow structure were measured by optical microscope. An air bubble was injected into the core section for better visualization. The measured inner diameter and outer diameter are 316μm and 759μm, respectively. Results indicate that the resulting inner diameter is greater than the fluidic value. The outer diameter is measured after the elution process, which peels away the ungelled outer layers of the printed fiber. The outer diameter after elution somewhat

Soft Matter Accepted Manuscript

Please do not adjust margins

corresponds to the location of the reaction front (i.e. modified $[G]_{\mathrm{cri}}$) described in Fig. 5d.

Table 1 shows a comparison between the experimental data and simulation results with different co-flow length. First, the experiment results indicate that the inner diameter is determined not only by the fluid dynamics, but also by a continuous expansion profile in the direction of the flow. Second, the transient inner diameter at the outlet of the fiber expands by approximately 70μm as compared to the initial fluid dynamics value. Thus, the shrinkage should not be neglected. Finally, compared to measured values, the relative mean error of the simulated inner diameter was less than 8%, proving that the weak coupling multi-physics model is reliable to estimate the transient inner diameter in the co-flow reaction process.

As shown in Table 1, the residual sol thickness indicated an identical trend to that demonstrated by R-r_{r}. In actuality, a small amount of gel must exist in the elution portion as well as some sol is maintained in the crosslinked network; once the generated gel achieves a certain concentration, higher level than that of the solubility of the gel, the new reaction region would fix on the gel matrix. Therefore, the relatively large differences between elution results and calculated values (R-r_{r}) imply the necessity of another concentration isogram which can be used to characterize the theoretical residual sol thickness.

5.4 Significance and Limitations of the concentration isogram

Unlike other parameters analysed in previous literature, such as general resident time, pressure gradient, etc., this work focus on the concentration isogram, which is a typical characteristic of the reaction-diffusion process. The concentration isogram plays a crucial role in ascertaining the validity of the simulation. The peak position of the concentration isogram $[G]_{\mathrm{cri}}$ was set as the boundary between the deformation mechanisms. This not only theoretically explains the morphological evolution, but also concerns the accurate prediction of the inner diameter as an integral boundary.

It is necessary to maintain a certain amount of residual sol on the fiber surface. The extrusion of hydrogel hollow fiber is usually the first fabrication step, such as is involved in the formation of a vascularized tissue engineering scaffold, followed by a typical mode of additive manufacturing that can generate a physical model layer-by-layer[24-26]. The key issue of component units is whether powder or fiber is quick and firm bonding. Once the alginate sol is completely gelled, the surface is elastic, smooth and extremely harmful to fiber adhesion during the construction of particular architectures, which has been detailed in many previous studies[27, 28].

Therefore, the adhesion between overlapping fibers is no longer negligible. Previous works[22,29,30] attempt to empirically control the flow rate to result in residual sol on the fiber surface, which has been proved to aid adhesion strength. In the present study, the concentration isogram analysis indicates a research strategy to theoretically estimate residual sol thickness, and future research will address the precision control of residual sol.

Tab.1 Comparison between the experimental data and simulation results with different co-flow length

Co-flow	Inner diameter /μm				Residual Sol Thickness /μm	
Length/mm	Fluidic Values $2r_0$	Coupling Values $2r_{\mathrm{s}}$	Experimental Values	errors	R-r_{r}	Elution results
5	245.6	260.8	270±10	3.4%	222	280
10	245.6	281.3	295±10	4.6%	138	165
15	245.6	315.7	320±8	1.3%	0	20

Conclusions

In this paper, a reactor-like spinneret is proposed to generate a continuous hollow hydrogel fiber. The spinneret possesses a transparent tube reactor to reliably control the deformation dynamics as well as aid online observing the morphological evolution. When changing the flow conditions, several co-flow states were generated: drag jetting, ejection jetting, and clogging. Additionally, an obvious expansion of core flow at the lower reaches of drag jetting was observed. The online observation just explains the huge difference between the theoretical value estimated by fluid dynamics and the experimental value of the inner diameter of the hollow fiber.

The obvious expansion of the core flow, i.e. the shrinkage of the shell portion, indicates that crosslink condensation should not be ignored. Based on a few simplifying assumptions and the weak coupling of the velocity field and diffusion-reaction of the co-flow, an intermediate state of the species concentration fields is obtained; the simulated results of the gel fraction gradient was in accordance with the SEM observation of the fiber cross section, which was of layered texture, and became gradually sparser from inside to outside. The typical sectional morphological evolution can be described according to a similar profile obtained by combining the initial fluidic radius and the critical concentration isogram $[G]_{cri}$ which triggers gelation and shrinkage. The experimental evidence indicates that the simulation is able to effectively predict the inner diameter of the hollow fiber. The transient inner diameter at the outlet (co-flow distance = 15mm) of the fiber

Soft Matter Accepted Manuscript

is expanded by approximately 70μm as compared to the initial fluid dynamics value, and the relative mean error of the simulated inner diameter was less than 8%. There were some limits in the estimation of residual sol thickness with the isogram $[G]_{cri}$, but also indicating a future research direction.

The proposed study provides a deeper insight and well control of geometry for hollow fiber printing which may potentially be used in thick tissue or organ fabrication. It may also provide a potential approach for other reacting co-flow processes, which permit quantifying the features of the reactants.

Acknowledgements

The authors gratefully acknowledge support from the National Natural Science Foundation of China (51475281, 51375292, and 51105239).

references

1 I. W. Sutherland, In Biomaterials: Novel Materials from Biological Sources; D. Byrom, Ed.; MacMillan Press: New York, 1991, 309-331.
2 D. A. Rees, PURE APPL. CHEM., 1981, 53, 1-14.
3 F. P. W. Melchels, M. A. N. Domingos, T. J. Klein, J. Malda, P. J. Bartolo and D. W. Hutmacher, PROG. POLYM. SCI., 2012, 37, 1079-1104.
4 A. Mendes, R. Lagoa and P. Bartolo, PROCEEDINGS OF THE 1ST INTERNATIONAL CONFERENCE ON ADVANCED RESEARCH IN VIRTUAL AND RAPID PROTOTYPING, 2003, 377-384.
5 E. Papajova, M. Bujdos, D. Chorvat, M. Stach and I. Lacik, Carbohydr. Polym., 2012, 90, 472-482.
6 J. L. Steinbacher, D. T. McQuade, J. POLYM. SCI. POL. CHEM., 2006, 44, 6505-6533.
7 A. Bhattacharyya, S. Dutta, P. De, P. Ray and S. Basu, Bioresour. Technol., 2010, 101, 9421-9428.
8 Y. Zhang, Y. Yu, H. Chen and I. T. Ozbolat, BIOFABRICATION 2013, 5, 25004.
9 D. Y. Park, C. H. Mun, E. Kang, D. Y. No, J. Ju and S. H. Lee, BIOFABRICATION, 2014, 6, 24108.
10 M. I. Santos, R. L. Reis, MACROMOL. BIOSCI., 2010, 10, 12-27.
11 Novosel, E. C.; Kleinhans, C.; Kluger, P. J. ADV DRUG DELIVER REV 2011, 63, 300-311.
12 M. Hu, M. Kurisawa, R. Deng, C. M. Teo, A. Schumacher, Y. X. Thong, L. Wang, K. M. Schumacher and J. Y. Ying, BIOMATERIALS 2009, 30, 3523-3531.
13 K. H. Lee, S. J. Shin, Y. Park and S Lee, SMALL, 2009, 5, 1264-1268.
14 T. Takei, N. Kishihara, S. Sakai and K. Kawakami, BIOCHEM. ENG. J., 2010, 49, 143-147.
15 M. Hu, R. Deng, K. M. Schumacher, M. Kurisawa, H. Ye, K. Purnamawati and J. Y. Ying, BIOMATERIALS, 2010, 31, 863-869.
16 O. Bonhomme, J. Leng and A. Colin, SOFT MATTER, 2012, 8, 10641-10649.
17 E. Kang, S. J. Shin, K. H. Lee and S. H. Lee, LAB CHIP, 2010, 10, 1856-1861.
18 A. S. Utada, A. Fernandez-Nieves, H. A. Stone and D. A. Weitz, PHYS. REV. LETT., 2007, 99, 94502.
19 P. Gacesa, CARBOHYD. POLYM., 1988, 8, 161-182.
20 T. Braschler, A. Valero, L. Colella, K. Pataky, J. Brugger, and P. Renaud, ANAL. CHEM., 2011, 83, 2234.
21 Y. Li, Y. Liu, S. Li, G. Liang, Y. Zhang and Q. Hu, Huagong Xuebao/CIESC Journal, 2014, 65, 5090-5096.
22 Y. Li, Y. Liu, S. Li, G. Liang, C. Jiang and Q. Hu, J. BIOSCI. BIOENG., 2016, 121, 111-116.
23 Y. Zhang, Y. Yu, A. Akkouch, A. Dababneh, F. Dolati and I. T. Ozbolat, Biomater. Sci., 2015, 3, 134–143.
24 G. I, In Additive Manufacturing Technologies: Rapid Prototyping to Direct Digital Manufacturing; Springer: Berlin, 2010.
25 D. W. Hutmacher, S. J Cool, CELL MOL. MED., 2007, 11, 654-669.
26 M. T. Arafat, I. Gibson, and X. Li, RAPID PROTOTYPING J., 2014, 20, 13-26.
27 S. Ghorbanian, M. A. Qasaimeh, M. Akbari, A. Tamayol and D. Juncker, BIOMED. MICRODEVICES, 2014, 16, 387-395.
28 C. Colosi, M. Costantini, R. Latini, S. Ciccarelli, A. Stampella, A. Barbetta, M. Massimi, L. C. Devirgiliis and M. J Dentini, MATER. CHEM. B, 2014, 2, 6779-6791.
29 S. Li, Y. Liu, Y. Li, Y. Zhang and Q. Hu, CHEM. ENG. PROCESS, 2015, 95, 98-104.
30 Q. Gao, Y. He, J. Fu, A. Liu and L. Ma, Biomaterials, 61, 203-215.

Soft Matter Accepted Manuscript

This journal is © The Royal Society of Chemistry 20xx